PHILOSOPHICAL TRANSACTIONS OF THE ROYAL SOCIETY A MATHEMATICAL, PHYSICAL & ENGINEERING SCIENCES

Excitations and excitons in photosystem I

G. S. Beddard

Phil. Trans. R. Soc. Lond. A 1998 **356**, 421-448
doi: 10.1098/rsta.1998.0174

The Royal Society

Excitations and excitons in photosystem I

By G. S. Beddard

School of Chemistry, University of Leeds, Leeds LS2 9JT, UK

The elementary requirements for energy transfer in a photosynthetic antenna are discussed. Energy migration between chlorophyll molecules in the PSI antenna reaction centre complex was modelled using a geometry based on the recent X-ray structure. The migration is trap-limited and an intrinsic electron transfer rate constant of 1.3 ps^{-1} was obtained by modifying the model to account for experimental results obtained from antennae of different sizes. Exciton coupling between pairs of Chlorophyll molecules was calculated and it is found that to prevent self-quenching their interplanar separation must be greater than or equal to 5 Å. In the PSI reaction centre, exciton coupling between adjacent chlorophylls was found to be around 300 cm^{-1} with no particularly large value between the special pair being necessary to describe the experimentally observed transient spectra of P_{700}^{+}–P_{700} and A_0^{-}–A_0. Electrochromic interaction is particularly important in reproducing the A_0^{-}–A_0 spectrum.

Keywords: photosystem I; reaction centre; energy transfer; antenna; electron transfer; exciton coupling

1. Introduction

The primary steps in photosynthesis take place in pigment protein complexes. These are classed as antennae in which numerous chlorophyll (Chl), or bacteriochlorophyll, molecules act so as to transfer absorbed light to the reaction centre (RC) where charge separation begins. The reaction centres studied so far contains six chromophores (chlorophylls and/or pheophytins) and secondary electron acceptors such as quinones or iron sulphur centres. The geometry and to some extent the energy of the Chl molecules is determined by the protein scaffold. The structure of several proteins containing reaction centres (Huber 1989; Krauss *et al.* 1996) and antennae (Tronrud *et al.* 1986; MacDermott *et al.* 1995) have been solved by X-ray- or electron-diffraction methods (Kuhlbrandt *et al.* 1994). Many picosecond and femtosecond studies have been carried out on the bacterial reaction centres as these pigment proteins may be isolated from their antennae (Breton *et al.* 1988; Zinth *et al.* 1995; Wynne *et al.* 1996). In green plants the PSII (Hastings *et al.* 1992) and PSI (White *et al.* 1996*a*) reaction centres and their antennae cannot be so well separated. The structure of PSI (Krauss *et al.* 1996), for example, shows that the antenna and reaction centre form an integral structure (figure 1). Fewer ultrafast laser studies have been reported on this RC than its bacterial counterparts. These experiments suggest that not only are the antenna pigments and those in the RC closely coupled by energy transfer, but also that electron transfer is trap-limited (Shuvalov *et al.* 1986; Hastings *et al.* 1994, 1995*a*, *b*; Kumazaki *et al.* 1994; White *et al.* 1996*a*). Furthermore, in trap-limited electron transfer it is difficult to determine the intrinsic rate constant and

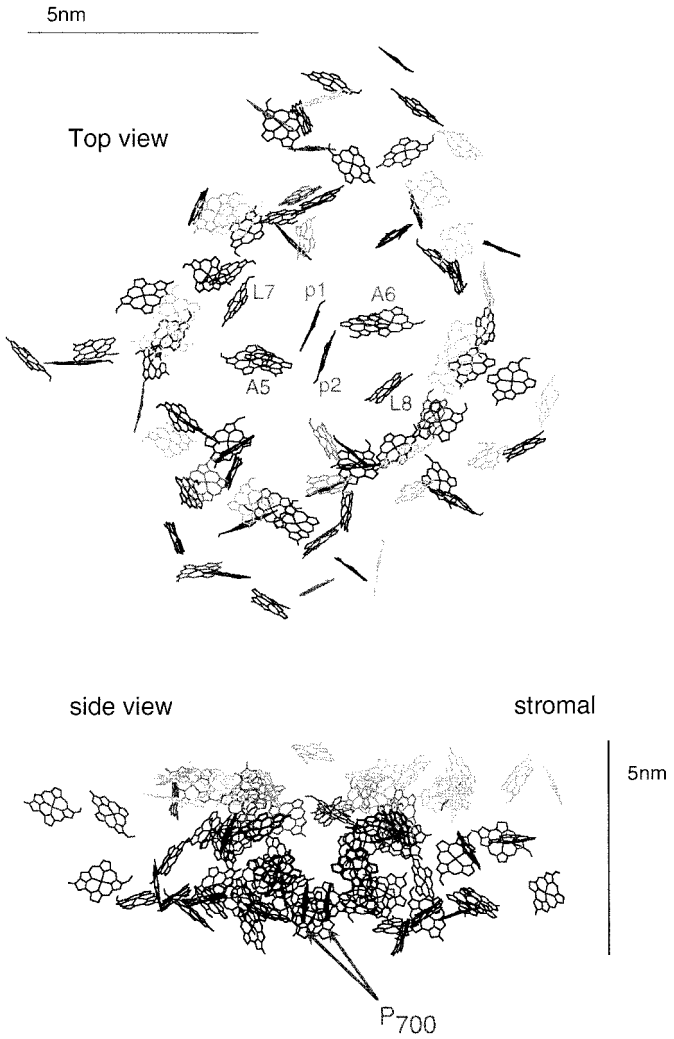

Figure 1. Two views of the PSI antenna complex. The Chl molecules have been superimposed on the basic PSI structure by matching the positions of the N atoms. The orientation of the Chl in the plane of the molecule is arbitrary. (*a*) Looking down onto the stromal side of the membrane, the iron sulphur centres are not shown but would be above the plane of the paper. The reaction centre complex is seen in the centre of the structure. The P_{700} 'special pair' are labelled $P1$ and $P2$, the accessory Chls, $C3$, $C4$ are not labelled but are adjacent to the acceptors $A5$ and $A6$, respectively. The 'linker' molecules are $L7$ and $L8$. (*b*) Side view. The P_{700} 'special pair' is seen edge on, in bold outline and towards the base of the protein. The molecules near to the stromal side of the membrane (top in (*a*)) are grey, those lower down are black.

this had to be estimated using a model of the antenna and reaction centre (White *et al.* 1996*a*).

The geometry of the antennae, as revealed by X-ray crystallography, exhibit several different designs and therefore the important parameters needed for an efficient antenna are considered first. This is followed by a section in which the geometry of PSI antenna-reaction centre complex is used to evaluate the energy migration characteristics and so determine the intrinsic rate constant of electron transfer. Finally the exciton structure of the PSI reaction centre pigments is described.

2. Antenna design

The arrangement of pigments recently observed in the LHII light harvesting complex of *Rps. Acidophilia* (MacDermott *et al.* 1995) at 2.5 Å resolution has a ninefold symmetry and consists of two concentric rings of bacteriochlorophyll (BChl) molecules, 27 in total (figure 1*a*). The accompanying LHI protein contains a ring of 16 pairs of BChls inside which is the RC. The LHII proteins are arranged outside this structure. A related antenna complex with eight-fold symmetry has also been observed (Koepke *et al.* 1996; Hu *et al.* 1997). In contrast to these, the X-ray structure of PSI appears to be very much more random in the arrangement of the 89 chlorophyll (Chl) molecules measured so far by X-ray crystallography (figure 1) (Krauss *et al.* 1993, 1996; Fromme *et al.* 1996). The structure is like that of a hollow cylinder inserted through an oblate ellipsoid. The cylinder has, very approximately, 20 Chl on its outer surface but is not completely hollow as it contains the six pigments forming the core reaction centre. There are also two 'linker' Chls (*L*7, *L*8, figure 1) that are between the reaction centre and the cylinder of Chls.

An antenna that might be considered as intermediate in order between the two extremes of LHII/I and PSI, is that of the FMO protein (Fenna & Matthews 1977; Tronrud *et al.* 1986), in which the seven Chls are situated around the surface of a bowl, six around the edges and the seventh at the bottom, the top is open (figure 2*b*); an eighth molecule, if it were present, could cap the bowl. This protein aggregates to a symmetric trimer and the interaction between monomers is described by exciton coupling (Mourik *et al.* 1994). A fourth type of antenna is that of chlorosomes where approximately 10 000 BChl-c are associated with approximately 10 RCs. There is still dispute as to the role of polypeptide in binding the chloropylls in this huge antenna. Some authors (Feick & Fuller 1984; Zuber 1986) describe five to eight BChl associated with each M_r3700 protein while others prefer the Chl to be aggregated and floating freely in the lipid (Noort *et al.* 1997).

The BChl in LHII (figure 2*a*) have absorption maxima at about 800 and 850 nm. There is of course not only rapid interpigment energy transfer around each ring but also from the *B*800 to *B*850 rings of molecules. The *B*850 ring has the BChl in van der Waals contact, with Mg–Mg distances of 8.7 Å for each pair and a distance of 9.7 Å to the next pair (MacDermott *et al.* 1995) (figure 2*a*). The Q_y dipoles in the LHII are arranged approximately head to tail to one another around the ring, the lower ring of BChl is arranged similarly facilitating strong exciton coupling within a ring. The spatial extent of the *B*850 exciton is uncertain as yet but estimates are that it spreads over two but not more than five molecules (Jiminez *et al.* 1996).

In PSI (figure 1), the orientation of the dipoles is not entirely known; the plane of each molecule is defined (±10%) but the dipole orientation within that plane is not, as the X-ray resolution is 4.5 Å (Krauss *et al.* 1996). In this antenna the dipole–dipole coupling between molecules is smaller than in LHII as the molecules are not arranged in such an ordered manner and the average near neighbour distance is a little larger at approximately 11 Å

The wide differences in the antenna structures are at first sight somewhat surprising and again (Zuber 1986) prompt questions as to what are the characteristics of an efficient light harvesting antenna. The two most-important properties would appear to be: (a) that an antenna should have a maximal cross section for light absorption over as wide a spectral range as possible; and (b) to be able to transfer this absorbed energy to the reaction centre trap but with minimal losses. A further requirement, (c), should be that the antenna must be able to function with repeated excitations

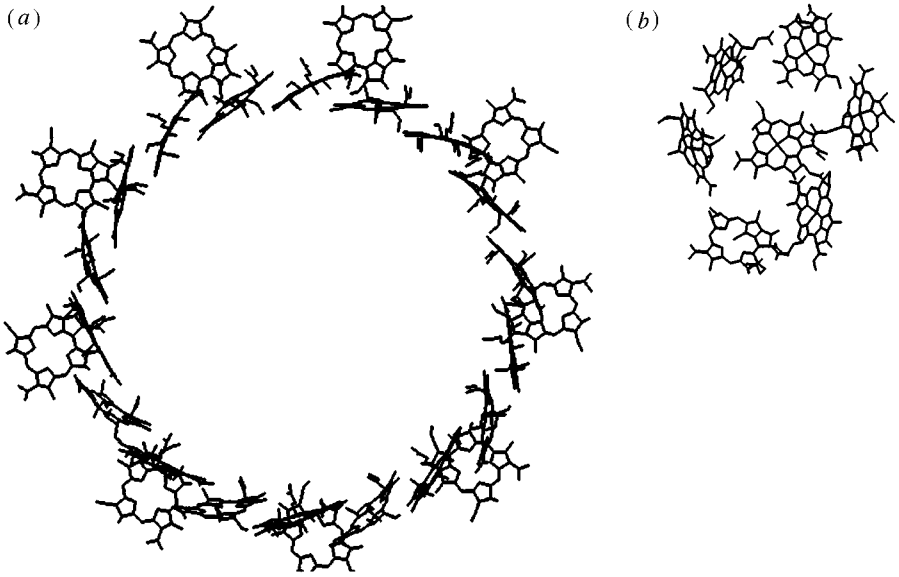

Figure 2. (*a*) X-ray structure of the antenna chlorophyll pigments of LHII (MacDermott *et al.* 1995), the *B*850 pigments are side on, the *B*800 face on. (*b*) A monomer of the FMO trimer (Tronrud *et al.* 1986). The central molecule is on the base of the bowl-shaped structure. Both structures are based on PDB files but are only approximately on the same scale.

without photochemical degradation for as long as possible. Carotenes, which are often found positioned intimate to the Chl (MacDermott *et al.* 1995; Kuhlbrandt *et al.* 1994), are one way to fulfil this requirement by efficiently quenching Chl triplet states but, additionally, there are also biochemical repair mechanisms.

In PSI the maximum cross section is achieved by perturbing the Chl-a molecules which have absorptions from approximately 667 nm, similar to that in an organic solvent, up to approximately 710 nm, an 840 cm^{-1} shift. In some species, e.g. Spirulina, the absorption extends to 740 nm, some 850 cm^{-1} below the trap at approximately 700 nm (Shubin *et al.* 1995). Spectra are similarly perturbed in other types of antenna. The precise type of the perturbation causing these spectral shifts is unknown for each molecule but could take one of several forms, i.e. exciton coupling between nearby Chl molecules; ligation to the Chl's Mg atom by basic molecules such as histidine on the polypeptide (Webber *et al.* 1996); bending the plane of the Chl molecule as in LHII; conformational changes of the Chl acetyl group (Parson & Warshel 1987) or electrochromic effects of nearby charges in the protein (Parson & Warshel 1987). The spread of absorptions compared to Chl in solution is very large and is supplemented in the bluer part of the spectrum by carotenes which transfer to Chl by energy transfer, and in some organisms by phycobilisomes which contain various types of allo- and phyco-cyanins (Pc) and exhibit efficient $Pc \rightarrow Pc$ and $Pc \rightarrow Chl$ energy transfer (Gantt *et al.* 1977; Zuber 1986; Huber 1989). Dimer, $(Chl)_2$, or aggregate formation could also cause a large broadening of the absorption spectrum by exciton interactions, but in Chl this usually leads to almost complete self-quenching (Beddard *et al.* 1976) via $(Chl^* \leftrightarrow Chl) \rightarrow (Chl)_2 \rightarrow Chl + Chl$, in preference to energy transfer, (the double arrow signifies energy migration). Using random walk methods (Beddard & Porter 1976) it has been estimated that Chl molecules must be greater than or equal to 10 Å apart to prevent this type of quenching, but a more detailed calculation given below shows that the planes of the Chl molecules must be greater than

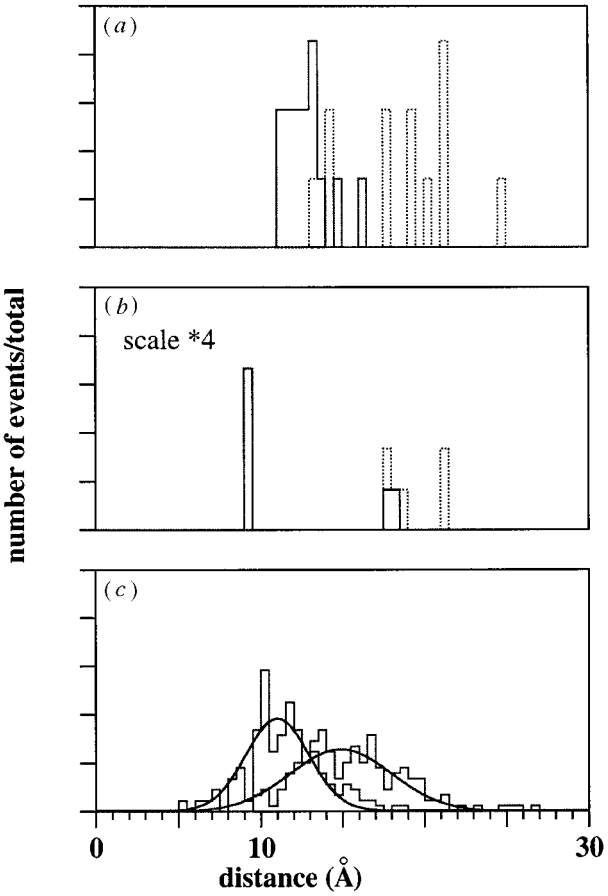

Figure 3. Histogram of the Mg–Mg distances (normalized to number of pigments) of first plus second, (solid line), and third plus fourth nearest neighbours (dashed line) for the antenna types (*a*) *FMO* (*b*) *LHII* and (*c*) PSI. In (*c*) a Gaussian fit to the distribution is shown that peaks at 11 and 14.8 Å. As the first and second distances significantly overlap, as do the third and fourth, these are plotted together.

or equal to 5 Å apart. Thus it is clear that in the antenna the molecules must be at least this far apart, if the Chl is undistorted, so as to facilitate rapid dipole–dipole transfer and prevent self-quenching. This seems to rule out having Chl freely disposed in lipid even though quenching may be partly ameliorated by mono- and di-galactosyl di-glycerides (Beddard *et al.* 1976) although Savikhin *et al.* (1994) take another viewpoint.

An estimate of the uniformity of the overall geometry can be obtained from the distribution of near-neighbour distances. In PSI the distribution of first and second near neighbour Mg–Mg distances has a maximum at approximately 10 Å (figure 3). In LHII the peak is at approximately 9.5 Å and in FMO it is 12 Å, each distance is consistent with our arguments about self-quenching.

The overlap integral for dipole–dipole energy transfer between Chl molecules (Grondelle 1985), produces a characteristic distance $R_0 \sim 80$ Å, which is very large with respect to the mean interpigment separation, $\langle R \rangle$, (i.e. $(R_0/\langle R \rangle) \gg 1$) and implies that transfer is possible, and is important, not just to the nearest neighbour but to others as well. Clearly in an antenna with a non-regular structure the connec-

tivity (bondedness) of energy migration paths involving only near neighbours must be poor and migration would soon become slow, if not impossible, as only a few pathways to the trap would exist. In effect this would occur if $(R_0/\langle R\rangle) < 1$ and this is the implicit assumption of calculations using only near neighbour transfers. When $(R_0/\langle R\rangle) \gg 1$, which is the case considered here, a number approaching the maximum possible energy pathways to the trap is generated. This is implied by the narrow distribution of distances in figure 3, which shows that the first and second neighbour distribution overlaps with that of the third and fourth, which peaks at approximately 15 Å and which is still far less than R_0. The solid lines (figure 3*c*) are Gaussian fits to the PSI distributions with means of 11 and 14.8 Å and standard deviation of 1.9 and 3.1 Å, respectively. In PSI the total rate of transfer to the nearest four molecules accounts for almost all of the rate compared to that when transfer from each one of the molecules to all others are considered. In LHII (figure 3*b*) the distributions are effectively delta functions at 9.5 and 18 Å and those of FMO (figure 3*a*), while less well defined, as only seven molecules are present, peak at approximately 12 Å and 20 Å, both sets of which are also consistent with rapid energy migration and preventing self-quenching.

The second way to achieve a large ratio $(R_0/\langle R\rangle) \gg 1$ would be to make $\langle R\rangle$ small. This is what occurs in carotene to Chl energy transfer where the molecules are in van der Waals contact with one another. The R_0 value is smaller, approximately 50 Å, (Grondelle 1985) than for Chl–Chl transfer, however, this is not primarily the reason for the closeness but it is that the transfer has to compete with the non-radiative decay of carotene excited singlet state, the lifetime of which is approximately 1 ps, as the transfer rate depends inversely on the donor excited state lifetime.

The antenna absorption cross-section can be increased by increasing the number of chromophores, either by using different pigments as in phycobilisomes or modifying Chl absorptions as in PSI, PSII and bacterial antenna. It is not completely clear what determines the maximum size of an antenna, sizes range from a few tens of Chls such as LHII to thousands as in chlorosomes. If all N pigments are of the same type then a single trap's population is $1/N$ if transfer to the primary acceptor is slow compared to energy migration, i.e. excited state equilibrium is reached prior to trapping. Increasing N clearly reduces the chance of trapping per unit time and allows fluorescence or non-radiative pathways to become relatively more important. As realized by Seely (1973) many years ago a funnel arrangement of pigments, such that on average pigments with lower energy transitions are placed closest to the trap, will reduce the antenna's effective size. The lower energy pigments act as partial traps and spatially localize the excitation. A good example is given by phycobilisomes where pigments might be arranged as hemispherical shells (Gantt *et al.* 1977) or as discs along rods connected at their base (Zuber 1986). In a hemispherical shell geometry, if a shell thickness is small compared to its radius after relatively few energy-transfer events the energy encounters the shell of lower energy absorbing pigments which act as a large effective trap. Thus we might expect to see many more pigments in phycobilisome antennae than in 'normal' antennae, such as in PSI or PSII, since the effective trapping rate remains large. Besides this spectroscopic issue there may also be, in some antennae, a geometric-to-kinetic effect, helping the antenna. With a large overall antenna composed of many separate proteins adjacent to one another maximizing energy transfer from one protein to another becomes paramount. This can be achieved by making the Chl–Chl transfer within one protein as fast as possible, for example in LHII where exciton coupling between molecules is

large. In effect it does not matter which Chl is closest to the next protein, say for LHII to LHI or LHII to LHII transfer, as the energy will rapidly reach the closest point from wherever it was initially placed either by absorption or by transfer from a Chl in another protein. This explains the advantage of having a structure in which there are a small number of closely but symmetrically placed Chls, and also allows variability in the number and relative disposition of pigment protein complexes depending on growth conditions.

A final point to consider is the increase in cross section of an antenna with many Chls compared to those with few. This is a straightforward one of numbers but the effect of spreading the absorption wavelengths is not so clear. In PSI for example the total antenna cross-section compared to the same number of Chls at 667 nm, the unperturbed absorption maximum wavelength, is only different by 3%, hardly enough in itself to account for the need for the spread in wavelength. The driving force is, presumably, that comparatively few photons arrive per nm per second from the solar spectrum thus widening the absorption band allows greater chance of capturing a photon *per se* but also over that of a competing organism. This would indicate that the spectral funnelling is a secondary and bonus effect of widening the antenna absorption.

The role of protein can be summarized a far as energy migration is concerned as: (a) it acts to keep the Chl molecules apart but at the correct relative orientation and separation to allow rapid energy transfer among numerous pathways from the point of excitation to the trap; and (b) the protein modifies the Chl absorption spectrum, for example via electrostatic fields, or the amino acid ligand attached to the Mg atom to produce a range of absorption wavelengths so maximizing the absorption cross-section. Exciton interaction between Chl molecules in the antenna should only occur if, simultaneously, a way is found to prevent self-quenching between pairs of Chls.

Energy migration and trapping in the PSI antenna reaction centre complex are now examined in more detail and this is followed by a description of the exciton coupling between pairs of Chl molecules in the reaction centre.

3. Trapping in PSI

Recent experiments (White *et al.* 1996*a*) attempted to measure the intrinsic rate constant of primary electron transfer (k_1) in the PSI antenna reaction centre complex (ARCC). It was found that the energy transfer was coupled to the electron transfer in the sense that the energy transfer was trap-limited, which is to say, a pseudo-equilibrium is established between the antenna and the trap prior to significant electron transfer. This is illustrated in the scheme below and is familiar to the simple kinetic description of bimolecular reactions in solution, but here, of course, it is the energy that diffuses not the molecules:

$$A^* \underset{k_{-a}}{\overset{k_a}{\rightleftharpoons}} P^*_{700}A_0A_1 \overset{k_1}{\rightarrow} P^+_{700}A^-_0A_1 \overset{k_2}{\rightarrow} P^+_{700}A_0A^-_1.$$

In this scheme the gross simplification that A represents all the antenna which transfer energy to P_{700} is made. Single average rate constants k_a and k_{-a} link A to P_{700}. The measured rate constant for $P^+_{700}A^-_0$ formation would be

$$k_q = \frac{k_a k_1}{k_{-a} + k_1}. \tag{3.1}$$

In the trap limit when $k_{-a} > k_1$, and a pseudo-equilibrium is established between the antenna and P^*_{700}. In the diffusion limit, electron transfer is comparatively fast; $k_1 > k_{-a}$ and thus $k_q = k_a$.

The experimental data (White *et al.* 1996*a*) could be fitted equally well to either of these two limiting cases and it was found necessary to use a calculation based on the partial antenna geometry of the 40 molecules known at that time (Krauss *et al.* 1993) to determine which of these two cases applied. We have now improved upon this calculation by using the positions of the 89 molecules in the 4.5 Å X-ray geometry of Krauss *et al.* (1996). As the details of the calculations are published elsewhere (White *et al.* 1996*a*) they are only summarized here. A master equation matrix of the rate constants of energy transfer by Förster (dipole–dipole) interaction was constructed and described energy transfer between each molecule and every other. Trapping of P^*_{700} by A_0 was included by assuming values for k_1 ranging from 0.001 to 100 ps^{-1}. The eigenvalues and eigenvectors of the equations were calculated and the excited-state population of each molecule evaluated as a function of time. The experimental data were simulated by summing the weighted decay profiles as appropriate to their absorption spectrum at the probing and exciting wavelengths chosen. Several models of the spectral distribution of pigments in the antenna were studied as well as a model in which the geometry was altered by deleting the linker Chls, ($L7$, $L8$) (figure 1).

Figure 4 shows a calculated decay profile together with some data of the decay of the antenna population taken by exciting with 150 fs pulses at 708 nm (White *et al.* 1996*a*) and probing at 690 nm. Similarly figure 5 shows the transient rise and fall of A_0^- population compared with the rather noisy data. This data are the third difference between flash and pre-flash experiments after subtraction of the long time transients as outlined in White *et al.* (1996*a*). A satisfactory fit to both sets of data is obtained with $k_1 = 1\ \mathrm{ps}^{-1}$. These data were calculated by assuming that there was a funnel of pigments in the antenna. The measured PSI absorption spectrum was matched by assuming Chl pigments (Shipman & Housman 1979; Jia *et al.* 1992) were absorbing at 667, 677, 687, 692, 697 and 712 nm. The number of pigments at each wavelength was 24, 26, 17, 13, 5 and 4, respectively. Furthermore P_{700} ($P1$, $P2$, see figures 1 or 10) was assigned to 697 nm, the accessory Chls ($C2$, $C3$) to 692 nm and primary acceptors A_0 and A'_0 ($A5$, $A6$) to 687 nm. The 712 nm Chl were set to the four antenna Chls nearest to the RC. The other pigments were assigned wavelengths arbitrarily but with the general rule that the further away from the trap the shorter was the wavelength. The result of this is that the ring of Chls around the RC contains molecules absorbing primarily at 687 nm with a few at 692, 677 and 667 nm. Which of these pigments are assigned to which wavelengths within this general arrangement does not seem to matter too much. In figures 4 and 6 the antenna data have an initial rapid decay which lasts for approximately 4 ps then the decay is essentially exponential due to trapping by P_{700}. The short time feature, which might be a rapid decay or rise of population, is the result of energy redistribution in the antenna and is virtually independent of the value of k_1 but depends on the excitation and probing wavelength (figure 6); for example, exciting at 700 nm, but probing at 660 nm or 710 nm produces initially a rapidly increasing antenna population as it takes some time for energy to reach the 660 nm absorbers not excited directly at 700 nm. The 710 nm pigments get some direct excitation but their decay into the traps is overwhelmed by transfer from other pigments resulting in an increasing population. Similar reasoning applies to excitation at 660 nm. This

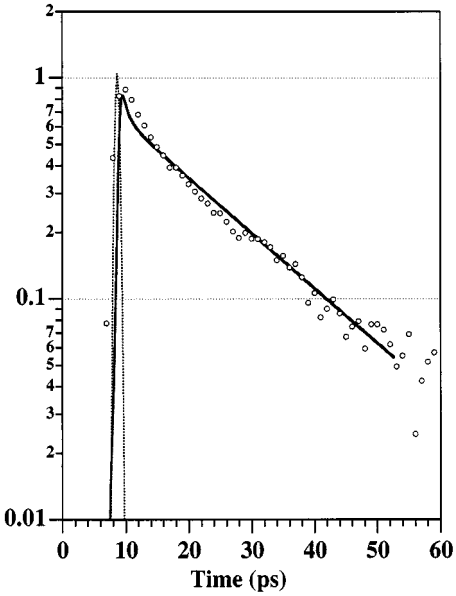

Figure 4. Experimental (points) and calculated decay antenna fluorescence decay normalized in intensity. The calculated decay assumes an electron transfer rate constant of 1 ps^{-1} and is convoluted with the laser profile (dotted) to simulate the data which was excited at 708 nm and probed at 690 nm.

contrasting behaviour at the same probing wavelength but with extreme exciting wavelengths is understandable as the same Chl molecules do not simultaneously absorb to any great extent at both these extreme wavelengths and it takes a little time for energy redistribution to occur. The top-most trace in figure 6 shows the decay for the antenna without a funnel. In this case it is not possible to distinguish energy redistribution from trapping as all molecules are spectrally identical and the decay is exponential.

Excitation directly onto the trap ($P1$, $P2$, figure 1) causes the six RC molecules to be excited within approximately 600 fs, energy then transfers onto the cylinder of surrounding molecules and subsequently flows back into the trap and into the red-most 712 nm absorbing antenna molecules. These remain the most populated at times greater than about 5 ps after excitation, this is true irrespective of where on the antenna the excitation was initially placed. This can be illustrated by plotting the residence probability (rp) of being on the trap versus time for different initial excitation positions in the antenna. When the trap is excited, but the trapping rate $k_1 = 0$, the rp (figure 7, curve a) falls steadily as energy transfers to and from the other RC Chl molecules (0 to approximately 600 fs), it then falls more rapidly as the trap becomes further depopulated by energy spreading into the remainder of the antenna. After approximately 5 ps the trap population becomes constant as energy is flowing back and forth from the antenna as equilibrium is established. When a peripheral molecule is excited initially the rp of the trap is zero but rises as energy flows into P_{700} (figure 7d). Again by approximately 5 ps an equilibrium is reached and the rp is independent of where excitation was initially placed. When trapping occurs, $k_1 \neq 0$, then the rp must always be less than when $k_1 = 0$ but only after approximately 5 ps does trapping dominate. This is most clearly seen in the average rp curve (figure 7f).

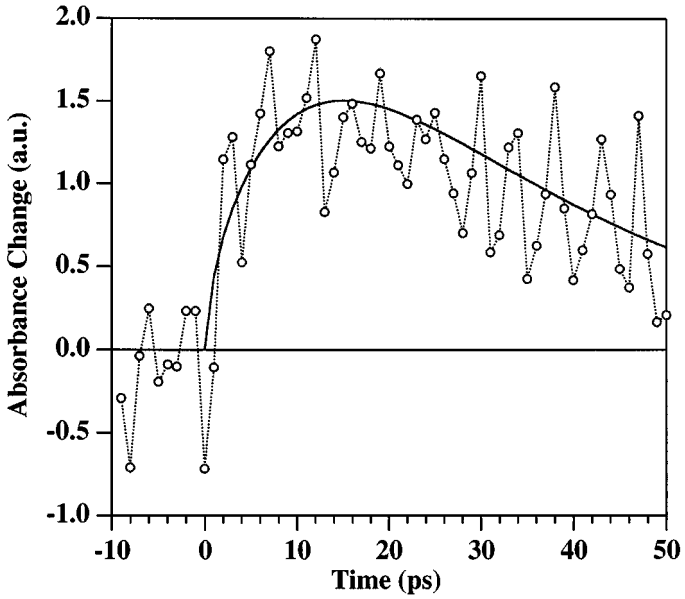

Figure 5. Calculated and experimental data (points) for the rise and decay of A_0^-. The solid line was calculated with the model described in the text, $k_1 = 1\ \mathrm{ps}^{-1}$, $k_2 = (\frac{1}{25})\ \mathrm{ps}^{-1}$.

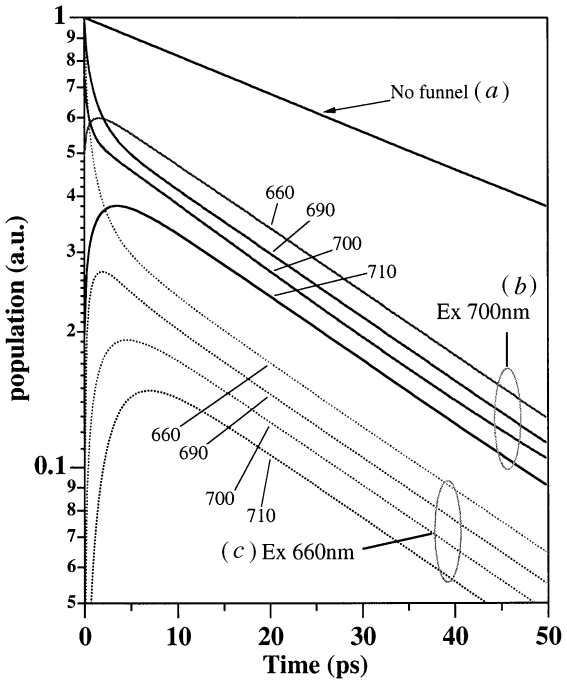

Figure 6. Comparison of calculated antenna decays with a trapping rate constant of $k_1 = 1\ \mathrm{ps}^{-1}$ for: (*a*) a spectrally flat antenna; (*b*) excited at 700 nm; and (*c*) excited at 660 nm. The probe wavelengths are as shown in the figure. These decays have not been convoluted with any experimental laser profile and are calculated at an exact wavelength, rather than a spread of wavelengths as is present experimentally, consequently the initial rising and falling transients are exaggerated over those expected in an experiment.

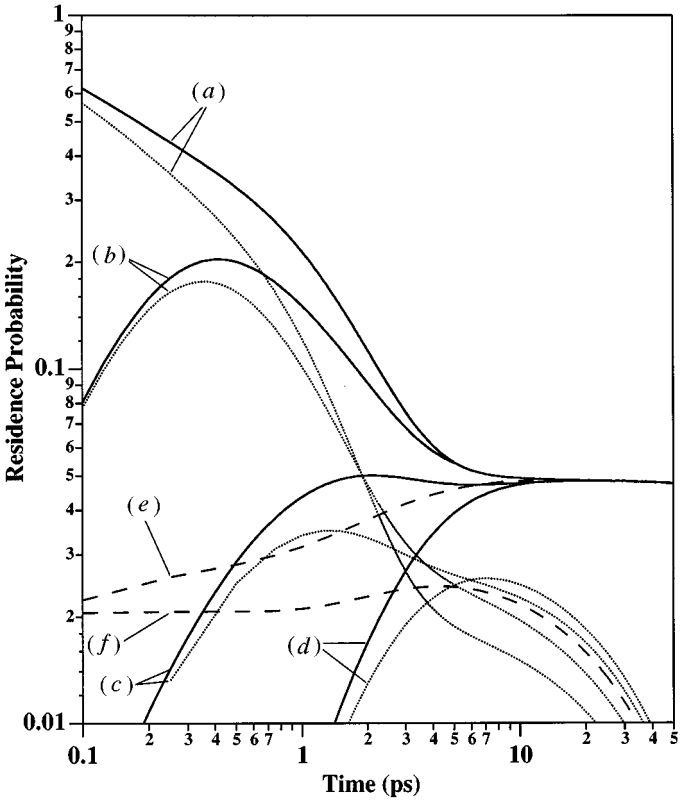

Figure 7. Residence probability of being on the P_{700} trap (averaged over both molecules) versus time for a funnel model. Solid lines with $k_1 = 0$, i.e. no trapping, and dotted line with $k_1 = 1\ \mathrm{ps}^{-1}$. (*a*) Initial excitation on the trap; (*b*) on *A*5 (see figures 1 and 10); (*c*) on an antenna molecule near to the *RC*; (*d*) on a remote molecule in the antenna. The dashed lines show (*e*) the average value when $k_1 = 0$ and (*f*) when $k_1 = 1\ \mathrm{ps}^{-1}$. Curves (*c*) and (*d*) show the limits of the *rp* when just the antenna is excited.

The energy migration around the antenna also has a spatial effect. Excitation on the periphery causes the energy to flow rapidly to nearby molecules and towards the trap. The excitation spreads all around the ring of Chl molecules surrounding the RC while remaining close to the trap and does not spread out again into the rest of the antenna. This effect is a consequence of the funnel and that quenching is in the trap limit. In the previous calculation on a reduced antenna size (White *et al.* 1996*a*; Beddard *et al.* 1995), each half of the antenna communicated badly with the other due to breaks in the pathways for energy transfer. This effect does not occur in the more complete X-ray structure. In an antenna with no funnel (i.e. spectrally flat), and no trapping, by approximately 4 ps the energy has spread over that half the antenna closest to the point of excitation. The antenna has become uniformly populated within 8 ps, independently of which molecule is initially excited. An approximate value of the energy diffusion coefficient at long times can be obtained from

$$D = \frac{1}{6n^2} \sum \sum r_{i,j}^2 k_{i,j},$$

which produces a value of $D = 2.47\ \mathrm{nm}^2\ \mathrm{ps}^{-1}$ and is similar to those observed for energy transfer in columnar liquid crystals ($2\ \mathrm{nm}^2\ \mathrm{ps}^{-1}$) (Markovitski *et al.* 1991)

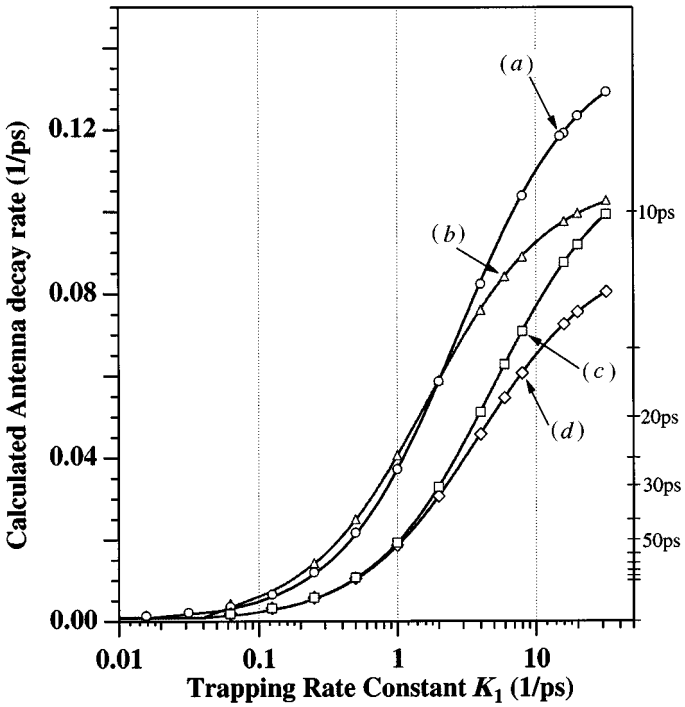

Figure 8. Calculated antenna decay rates versus trapping rate constant, k_1, for four antenna models. (a) funnel, (b) funnel without linker molecules, (c) spectrally flat, (d) spectrally flat without linker molecules. The lines through the points are fitted with equation (3.1).

and slightly larger than in some molecular crystals ($0.5\,\mathrm{nm^2\,ps^{-1}}$) (Kalinowski *et al.* 1997). The corresponding mean distance diffused ($\sqrt{(6Dt)}$) in 4 ps is 7.7 nm, about 75% of the lateral extent of the antenna. An average single-step jump time is 0.11 ps using the mean separation of the first four neighbours of 13 Å. The first four neighbours account for virtually all of the total energy transfer-rate constant.

A second calculation was done in which all pigments had the same wavelength, and as might be anticipated, the excited state decay time of the antenna was far longer than is the case with the spectral funnel (figure 8a). In fact k_1 has to increase by about three-fold to reduce the antenna decay to that of the funnel model. The variation of the calculated antenna decay rates with k_1 is shown in figure 8. The curves (a, c) fitted to the calculated data are equation (3.1) with $k_a = 0.143$ and $k_{-a} = 2.78$; funnel, and $k_a = 0.115$ and $k_{-a} = 4.94$; spectrally flat model. To understand why equation (3.1) fits the calculated antenna data, imagine that the energy migration is randomly jumping among the molecules in finding its way to the trap. This process is thus similar to the Brownian motion undergone by a molecule in solution before reaction. It is, however, somewhat surprising that with such a small number of molecules in the antenna equation (3.1) seems to hold. The effect of the spectrally flat antenna is to increase k_1 to approximately $7\,\mathrm{ps^{-1}}$ or at a fixed k_1 to increase the antenna decay time to approximately 40 ps from 20 ps. This is not a very great difference in terms of trapping yield. If we take a non-quenching antenna decay time of 1 ns then the trapping yield with and without a funnel is 98 versus 96%, a small difference. Therefore the value of the funnel seems to be rather limited in terms of trapping advantage but of more benefit in spectral coverage. However, in the case of a 'pathological' funnel, for example where the red-most pigments are not

near the trap, in an inverted type of funnel but with $k_1 = 1\,\mathrm{ps}^{-1}$, and the six trap pigments with the same wavelengths as in the normal funnel, the antenna decay time is significantly increased from approximately 20–90 ps or only 91% trapping yield.

To investigate the variation that the antenna size has on the antenna decay time the several sets of experimental data were taken from the literature. The calculated data were calibrated with these experimental values using the equations of Hemenger *et al.* (1972) and Pearlstein (1982), which describe energy migration and trapping on a lattice, equation (3.2). This approach improved the estimate of the intrinsic rate constant k_1. The parameters in this formula were calibrated with our simulation and then fitted the other published data from PSI antennae with various numbers (n) of chlorophylls. This was an attempt to overcome the difficulty of being unable to simulate energy migration on antennae with different numbers of molecules whose positions are unknown. However, the choice is restricted to antennae surrounding PSI type reaction centres so that they all have similar characteristics. This approach would not necessarily, for example, describe energy migration in LHII antenna.

Pearlstein gives the mean antenna lifetime τ_n in terms of the antenna size, n, as

$$\tau_n = \left(\frac{1}{k'_a} - \frac{1}{k'_J}\right)\left(\frac{(n-1)^2}{nq}\right) + \frac{\beta n}{k'_J} + \frac{k'_{-a}}{k'_a}\frac{(n-1)}{k'_1} + \frac{1}{k'_1}, \tag{3.2}$$

where k'_a, k'_{-a} and k'_1 are the Förster rate constants for trapping from the antenna, detrapping and charge separation, respectively, the superscripts refer to equivalent rate constants to those in equation (3.1). k'_J is the rate constant for mean near-neighbour inter-pigment jumps in the antenna and the constants, β and q for a cubic lattice are $\beta = 0.262$ and $q = 6$. The value of n used is the total number of antenna chlorophylls. Rewriting equation (3.2) in the form of equation (3.1) and if $k_n = 1/\tau_n$ then

$$k_n = \frac{k'_1/A_n}{B_n/A_n + k'_1}, \tag{3.3}$$

where

$$A_n = \left(\frac{1}{k'_a} - \frac{1}{k'_J}\right)\left(\frac{(n-1)^2}{nq}\right) + \frac{\beta n}{k'_J} \quad \text{and} \quad B_n = \frac{k'_{-a}}{k'_a}(n-1) + 1. \tag{3.4}$$

The values of the constants k'_a, k'_J and k'_{-a} can be obtained from fitting equation (3.3) to our simulation (figure 8). The funnel model with all 89 molecules present is fitted with $k_J = 1.3\,\mathrm{ps}^{-1}$ and $k'_a = 1.61\,\mathrm{ps}^{-1}$ and $k'_{-a}/k'_a = 0.48$. The first two values are not too different to those found for a 48 antenna model (White *et al.* 1996*a*), 1.01 and 1.43, respectively, but $k'_{-a}/k'_a = 0.21$ and this increased ratio in the larger antenna is a consequence of the increased number of molecules surrounding the RC and increasing k'_{-a}. The calculated inter-pigment jump time (Pearlstein 1982) of $1/q.k_a = 0.1$ ps is generally comparable to that suggested by Owens *et al.* (1987) and measured by Savikhin *et al.* (1994) and with the average time per jump taken in our simulation. The experimental and calculated data for PSI are shown in figure 9 where the literature set of antenna sizes has been normalized to the data of Shuvalov *et al.* (1986), as that paper reports experiments on a 70 molecule antenna, a size similar to that used in our calculation. After normalization all points should appear on the same curve. The sequential numbers on this figure are indexed in the figure legend. From this data the mean trapping rate constant is $1.25\,\mathrm{ps}^{-1}$. The data seems to fall into two groups with a separation between $k_1 = 1.5$ and 2. There is a well-defined group at around $k_1 = 1$ and a few points spreading out to larger k_1 values.

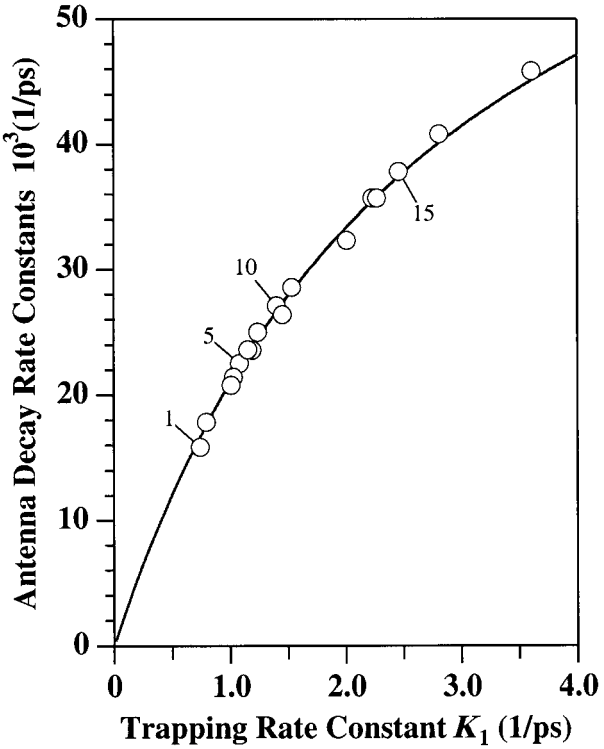

Figure 9. Observed antenna decay rates (circles) versus the corresponding calculated trapping rate k_1. The solid line is equation (3.3) normalized to the 70 Chl antenna of Shuvalov *et al.* (1986) point 8. Points 1 (Kamagowa *et al.* 1983), 2 (Lin *et al.* 1994), 3, 9, 12, 18, (Kumazaki *et al.* 1994), 4–7, 10, 17 (Owens *et al.* 1987, 1988), 8, (Shuvalov *et al.* 1986), 11 (White *et al.* 1996*a*), 13, (Lee *et al.* 1995), 14 (Wasielewski *et al.* 1987), 15 (Werst *et al.* 1992), 16 (Turconi *et al.* 1993; Holzwarth *et al.* 1993).

There does not seem to be a clear reason why these points have larger k_1 values but generally they come from experiments where there are large reported antenna sizes, more than 100 Chl, and comparatively short antenna decay times or where excitation intensities may lead to singlet–singlet annihilation.

It has been suggested (Krauss *et al.* 1996) that the so called linker Chls (*L*7, *L*8) (figure 1), that are between the main antenna and the RC can act, as their name suggests, to conduct energy from the antenna to the RC. On a purely numerical basis this seems unlikely as there are 16–20 Chls immediately surrounding the RC so the population of the two linkers will be only about 12% of these. However, if these linker molecules were the most red-shifted in the antenna this population will be increased, and as the linkers are closest to the RC, the transfer rate is further increased by the ratio of the sixth power of the mean separations. More precisely the antenna decays have been calculated with these two linker molecules removed and both with and without a spectral funnel. The results are shown in figure 8*b*, *d*, the fitted lines have $k_a = 0.107$ and $k_{-a} = 1.65$ (funnel model), and $k_a = 0.09$ and $k_{-a} = 3.86$ (spectrally flat model). In both cases k_a and k_{-a} are smaller than the corresponding values when all antenna molecules are included but k_{-a} is reduced relatively more than is k_a. Removing the linker Chls only increases the antenna decay rate by a marginal amount up to a k_1 value of approximately $2\,\mathrm{ps}^{-1}$ and as $k_1 \rightarrow \infty$, $1/\tau \rightarrow 0.107\,\mathrm{ps}^{-1}$ compared to $0.143\,\mathrm{ps}^{-1}$ for the complete antenna,

therefore, without the linker molecules the antenna is closer to the diffusion controlled limit. A similar effect occurs for the spectrally flat antenna.

4. Exciton coupling in the PSI reaction centre

The photosynthetic reaction centre both in bacteria and PSI contains six pigments and two secondary electron acceptors arranged in a well defined but approximate C2 symmetric structure in the protein. The electronic structure of the bacterial reaction centre has been the subject of several investigations (Parson & Warshel 1987; Scherer & Fischer 1989, 1997; Warshel *et al.* 1994; Alden *et al.* 1995, 1996; Thompson *et al.* 1991; Thompson & Zerner 1991; Thompson & Schenter 1995; Haran *et al.* 1996; Wynne *et al.* 1996), and because of the proximity of the chlorins has lead to 'supermolecule' descriptions of the excited states. The PSII reaction centre has been less extensively studied most notably by Durrant *et al.* (1995) using a structure modified from that of bacteria by increasing the special pair separation by 2.8 Å. They suggest a similar size of exciton coupling between each pigment and its near neighbour and exciton states partially delocalized over the pigments. In contrast, the PSI reaction centre does not appear to have been examined in such detail.

The structure of the PSI reaction centre is shown in figure 10, and while there is clearly a great similarity to that of the bacterial RC (Diesenhofer *et al.* 1984; Huber 1989) but there are also important differences. The most obvious is that of the accessory Chls ($C3$, $C4$) which are rotated about their y-local axis (see figure 11) compared to their bacterial equivalents, the other is that the pigments are all Chl-a not BChl and bacteriopheophytins. The linker Chls ($L6$, $L7$) are also shown and give the impression that they are very close by, but they are actually positioned in front of and behind the plane of the figure (see figure 1).

The absorption spectrum of the PSI RC was calculated by generating the MOs of the Chl, Chl^+ and Chl^- molecules, performing configuration interaction in the 'four-orbital' model as the major transitions involve the top two filled orbitals and the lowest two unfilled orbitals. The pairwise exciton coupling between each pair of molecules was then calculated using the self-consistent field/configuration interaction method described by Warshel & Parson (1987). In each pair interaction the off-diagonal terms in the configuration matrix describe the mixing of the local and charge-transfer transitions. These matrices were now combined and diagonalized to obtain the eigenvalues and spectrum of the complete RC. The spectra of six- and eight-molecule structures (by additionally including $L7$, $L8$ to the RC) was modelled and also the difference spectra P^+_{700}–P_{700} with one of the special pair as Chl^+ and A^-_0–A_0 with the acceptor as Chl^-. The orientation of the Chl molecules in the plane of the nitrogen atoms is unknown, the X-ray data are as yet not sufficiently precise, so that free rotation of the molecules in that plane was allowable and many orientations were examined to find those best representing the transient absorption data.

5. Method

The initial MOs were calculated using Gaussian-94 (Frisch *et al.* 1995), in an all-electron Hartree–Fock calculation using a 3–21G basis set. The atomic coordinates were taken from the X-ray structure of ethyl chlorophyllide.H_2O (Chow *et al.* 1974). The water is attached as a ligand to the Mg atom. The orbital symmetry for the top two occupied and lowest two unoccupied orbitals were the same as those reported

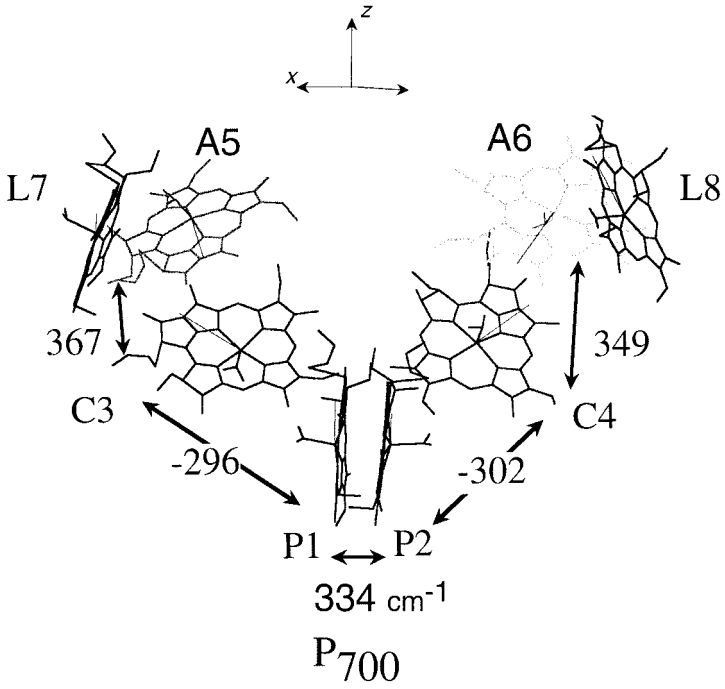

Figure 10. Geometry of the PSI reaction centre. The P_{700} special pair is labelled $P1$, $P2$, the accessory Chls, $C3$ and $C4$, the primary acceptors $A5$ and $A6$ and the 'linker' Chl $L7$ and $L8$. The exciton coupling energies (cm^{-1}) are also shown between nearest pairs of molecules. The thin line on the Chls show the direction of the Q_y dipole, water molecules are also shown attached to the Mg atoms which lie about 0.3 Å above the plane of the Chl.

by Nagashima (Nagashima *et al.* 1986). These orbitals give rise to four transitions (Gouterman 1978).

The wavefunction for the excited states of the Chl molecules is written as

$$\Psi_i = \sum_a c_{i,a}\psi_a, \tag{5.1}$$

where ψ_a represents the singlet wavefunction corresponding to an excitation from orbital j to k; and ψ_b that from orbital m to n, ψ_0 is the zero-order ground-state wavefunction, equations (5.3) and (5.4). The configuration interaction coefficients are $c_{i,a}$ and were calculated by solving the matrix equation (Warshel & Parsons 1987)

$$Ac_i = \Delta E_i c_i, \tag{5.2}$$

where ΔE_i are the excitation energy eigenvalues and the matrix A is given by

$$A_{a,a} = \langle\psi_{j\to k}|H|\psi_{j\to k}\rangle - \langle\psi_0|H|\psi_0\rangle = E_k - E_j + 2\langle jk|kj\rangle, +\langle jk|jk\rangle, \tag{5.3}$$

$$A_{a,b} = \langle\psi_{j\to k}|H|\psi_{m\to n}\rangle = 2\langle mk|nj\rangle - \langle mk|jn\rangle. \tag{5.4}$$

The matrix elements are calculated as

$$\langle mn|pq\rangle = \iint \varphi_m(1)\varphi_n(2)(1/r_{1,2})\varphi_p(1)\varphi_q(2)\,\mathrm{d}\tau_1\mathrm{d}\tau_2$$

$$\approx \sum_{s,t} v_{m,s}v_{n,t}v_{p,s}v_{q,t}\gamma_{s,t}, \tag{5.5}$$

$$\gamma_{s,t} = 3.77\times10^4\exp(-0.232r_{s,t}) + 1.16\times10^5/(2.82 + r_{s,t}), \tag{5.6}$$

Table 1. *Experimental and calculated spectroscopic parameters of chlorophyll monomers*

	calculated energy $\Delta E^{(\mathrm{est})}$ 10^4 cm^{-1}	observed energy 10^4 cm^{-1}	calculated strength D^2	observed strength D^2	calculated dipole angles to x-axis	observed dipole angles[d]
Bx	2.55	2.335	35	77[a]	11.5	3.7
By	2.25	2.335	65	77[a]	86.0	84.5
Q_x	1.76	1.73	6.3	4[b]	35.9	—
Q_y	1.49	1.51	26	32[a,c]	84.1	77.5

[a]Renge *et al.* (1993).
[b]By comparison with spectrum (Shipman & Housman 1979).
[c]Sauer *et al.* (1966).
[d]Zandvoort *et al.* (1995) averaged values and allowing for different axis directions.

where γ is an approximation to the electron–electron repulsion term (in cm^{-1}), $r_{s,t}$ the distance between atoms s and t (in Å), and v the MO expansion coefficients (Warshel & Parsons 1987).

The four local transitions are conventionally labelled Q_x, Q_y, B_x and B_y. Chlorophyll has its lowest $\pi\pi^*$ transition (Q_y) at 662 nm (in ether), a weaker Q_x band at 578 nm and the B_x, B_y transitions are found in a broad band at approximately 430 nm (Falk 1964). The eigenvalues from the initial *ab initio* calculation of the chlorophyll monomer produced transition energies (ΔE) larger than those observed experimentally. This discrepancy has been noted before, both for porphyrins and chlorins (Warshel & Parsons 1987; Petke *et al.* 1978). The calculated ΔE and experimental values could be matched by the formula $\Delta E(\mathrm{est}) = 0.684 * \Delta E - 1550$ (cm^{-1}). These estimated energies were used only for comparison of the calculated spectra with experiment. The transition dipole magnitudes and directions compared moderately well with experiment except for the angle of the B_x transition, table 1, however, the Q_y transitions are the most important for comparison of the exciton coupled spectra with experiment.

The exciton interaction was calculated between the four local states Ψ_i on molecule 'A' with states Ψ_j on molecule 'B' leading to eight new states. The monomer wavefunction, ϕ_1, or ϕ_2 in a dimer was constructed as for the initial molecules as a linear combination of orbitals

$$\phi_{1i} = \sum_s v_{i,s}\chi_s \quad \text{and} \quad \phi_{2i} = \sum_t v_{i,t}\chi_t, \tag{5.7}$$

except that labels s and t on the expansion coefficients v refer to different molecules, and χ is an orbital on atom s or t. The interaction matrix in the notation of Warshel & Parson (1987) is

$$U = \left(\begin{array}{cc|cc} \Delta E^a & U^{\mathrm{ex}} & U^{\mathrm{loc,ct}} & \\ U^{\mathrm{ex}} & \Delta E^b & & \\ \hline U^{\mathrm{ct,loc}} & & U^{\mathrm{ct}} & 0 \\ & & 0 & U^{\mathrm{ct}} \end{array}\right), \tag{5.8}$$

where U^{ex} is the 4×4 matrix of exciton interactions between molecules a and b, an element of which has the form

$$U^{\mathrm{ex}}_{i,k} = \langle \Psi^a_i | H | \Psi^b_k \rangle, \tag{5.9}$$

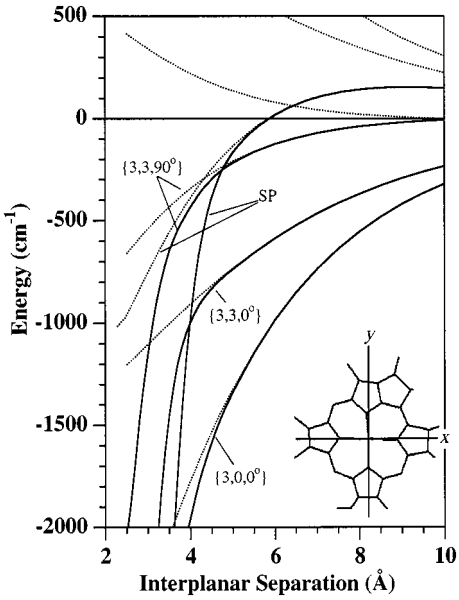

Figure 11. Exciton and CT coupling energy for Chl dimers placed face to face, displaced and separated according to the labels $\{x, y, \theta\}$, and displaced along a line perpendicular to the molecular plane, z-axis. The exciton and CT interaction energy is the solid line, the exciton energy alone the dotted line of each pair. The curves labelled SP are calculated using the P_{700} geometry but with the interplanar separation as shown between $P1$ and $P2$. In the RC, $P1$ and $P2$ are separated by 4.5 ± 0.5 Å (Fromme 1996).

and is evaluated by analogy to equation (5.5). $\Delta E^{a,b}$ are diagonal matrices of local transition energies. The pair of molecules also has four principle charge transfer (CT) interactions U^{ct} in which an electron is transferred from an orbital of one molecule to that of another. These transitions can also interact with the local transitions (Q_y, etc.) of the molecule, $U^{\mathrm{ct,loc}}$ (Warshel & Parsons 1987).

6. Chlorophyll dimers

Before describing the exciton coupling in the PSI RC the interaction between dimers is considered. This is relevant to our discussion of the quenching by pairs of Chls in the antenna. Figure 11 shows the energy of the lowest states between molecules, with exciton (dotted line) and CT plus exciton couplings (solid lines) and whose planes are parallel to one another but separated on the z- and displaced on the x- and y-axes. In the coordinate frame of the Chl molecules the local z-axis is perpendicular to the plane of the molecule and passes through the Mg atom. The y-axis goes approximately through two opposing N atoms one of which is in the ring adjacent to ring V, see insert in figure 11.

Many geometries were studied and it can be seen in figure 11, where only a few are shown, that as the molecules approach to within 5 Å the state with exciton and charge-transfer coupling (solid line) is lowest in energy. This is true for most of the face-to-face configurations when one ring is above or partly above the other. The data labelled SP are calculations done on the P_{700} special pair when one molecule is translated perpendicularly with respect to the other, but with the same relative orientation as in the RC (figure 10). The observed separation measured this way is 4.5 Å (Fromme 1996). The variation of energy of P_{700} with separation is similar to

that of the other geometries with the state containing CT character becoming lower in energy as the molecules approach one another.

The appearance of a low energy CT state for most geometries with a planar separation of less than or equal to 5 Å supports our previous arguments (Beddard *et al.* 1976; Beddard & Porter 1976) and those presented above that suggest that Chl self-quenches when the molecules get too close. This suggests that one reason Chl is bound to protein is to prevent self-quenching which would prematurely stop energy migration.

7. PSI reaction centre

The calculations on the PSI RC used the coordinates of the nitrogen atoms from the X-ray data and superimposed the Chl geometry (figure 10). The spectrum of PSI was calculated with all six molecules included. As a test the seventh and eighth linker Chls were added but these changed the spectrum only slightly and were not included in further calculations. The coupling to the linkers from A_0 ($A5$, figure 1) and A_0' ($A6$) is approximately 60 cm^{-1}. The additional energy due to charge transfer was found to be very small (less than 5 cm^{-1}) for all pairs of molecules except for the special pair (approximately 150 cm^{-1}), using a 'typical' protein dielectric constant of three. When included in the total calculation only a 2 nm shift in wavelength of the lowest transition was produced by this interaction. The PSI spectrum was calculated at several different orientations of the Chl molecules by rotating them in the plane of the N atoms. The angle between the special pair Q_y transitions in bacterial RCs is approximately 38° (Deisenhofer & Michel 1989) and a similar angle has been suggested for PSI (Webber *et al.* 1996). A rather *ad hoc* procedure was initially used as the spectrum of PSI was not known, only its difference spectrum. We started with an angle of 40° between the special pair and varied the angles of the accessory ($C3$, $C4$, figure 10) then the A_0 Chls ($A5$, $A6$) to produce a smooth looking spectrum peaking at the longest wavelength approximately 692 nm. At the same time the couplings between the left and right sides of the structure were kept about the same. The coupling values for the RC are shown in table 2 and figure 10. The spectrum of P_{700}^+ ($A5$ $C3$ $P1$ $P2^+$ $C4$ $A6$) (figure 11), and then A_0^- ($A5$ $C3$ $P1$ $P2$ $C4$ $A6^-$) was also calculated and subtracted from the neutral spectrum and compared to a normalized experimental difference spectrum. Spectra with $P1^+$ instead of $P2^+$ and $A5^-$ instead of $A6^-$ gave similar results. The in-plane angles in the neutral, P_{700}^+, and A_0^- structure were always the same and were simultaneously varied until a best fit to the experimental data were obtained. The angular range for good fitting is fairly wide for P_{700}^+ but much more restrictive for A_0^-, and was within ±10°.

It was found necessary to include electrochromic interactions in the P_{700}^+ and A_0^- difference spectra (P_{700}^+–P_{700}) and (A_0^-–A_0) to match the experimental data. This has a small but noticeable effect on P_{700}^+ but is essential to obtaining an A_0^- spectrum that models the experimental difference data. The interaction is added to the relevant diagonal terms in equation (5.8), before diagonalization, and takes the form (Parson & Warshel 1987)

$$\Delta(\mathrm{elec})_i^b = -\sum_n c_{i,a}^2 \sum_{s,t} v_{q,s}^2 (v_{a1,s}^2 - v_{a2,s}^2)\gamma_{s,t}/D. \tag{7.1}$$

This is the energy correction for the transition k on molecule b. D is the dielectric

Table 2. *Exciton coupling energies (to nearest* cm^{-1}*) for a model of* PSI *reaction centres based on the X-ray structure of Krauss et al. (1996)*

(The values in brackets are those energies when the RC contains either (P_{700}^{+}) or [A_0^{-}].)

	$P1$	$P2$	$C3$	$C4$	$A5$	$A6$
$P1$	0 (12)	334	−296	51	45	3 [80]
$P2$		0	86 (−222)	−303 (−248)	−3 (69)	−33 (68) [21]
$C3$			0	73	368	−20 [9]
$C4$				0	−28	367 [−44]
$A5$					0	18 [−58]
$A6$						0

In the notation of Krauss $P1 \equiv eC1'$, $P2 \equiv eC1$, $C3 \equiv eC2$, $C4 \equiv eC2'$, $A5 \equiv eC3$, $A6 \equiv eC3'$.

constant, a value of three was used, and the subscript label q refers to orbital q of atom s and depends on whether the transition involves P^{+} or A^{-}, see Parson & Warshel (1987) for details. The calculated spectra are shown in figure 12, and comparisons of the calculated and experimental difference spectra in figure 13.

The noticeable feature of the coupling (see table 2 and figure 10), is the similarity of the magnitude of the values between the pigments, electronically the identity of a special pair is not particularly obvious, unlike the bacterial RC where the coupling between the special pair is approximately 1500 cm^{-1} in *Rps. Viridis* and 2100 cm^{-1} in *Rb. Sphaeroides*, at 4.2 K (Small 1995), and which is also much stronger than that between the other pigments. In this respect the PSI RC is more similar to the PSII model of Durrant *et al.* (1995) excepting that in that model the couplings were much smaller. This smaller coupling in PSI is not entirely unsurprising as the plane to plane separation in bacterial RCs is approximately 3.5 Å, but 4.5 Å in PSI and possibly larger in PSII (Kwa *et al.* 1994). Table 2 also shows the coupling energies for the RC and for the RC with P_{700}^{+} and A_0^{-}. The main difference occurs between the charged species, P_{700}^{+} or A_0^{-}, and the adjacent pigment. In P_{700}^{+} this coupling is reduced to approximately $\frac{1}{30}$ of the value between $P1$ and $P2$ in P_{700}. The P_{700}^{+} spectrum (figure 12) shows this effect as it is narrower than the 'neutral' RC. A transition is also seen at approximately 820 nm due to Chl^{+} but is so weak and shifted that it does not affect the transitions in the 650–700 nm region. A similar transition is observed both in the experimental absorption spectrum of Chl^{+} and Chl^{-} (Fujita *et al.* 1978).

The differences in the calculated RC spectra (P_{700}^{+}, P_{700}^{+}, A_0^{-}) are explained by the changes in the coupling between pigments. In the P_{700}^{+} spectrum the two largest energy eigenvalues are more similar in energy than in the neutral RC, as electronically the structure has two similar halves of three pigments as the $P1$–$P2$ interaction is small. The spectrum of A_0^{-} is similar to that of the neutral RC as only the coupling

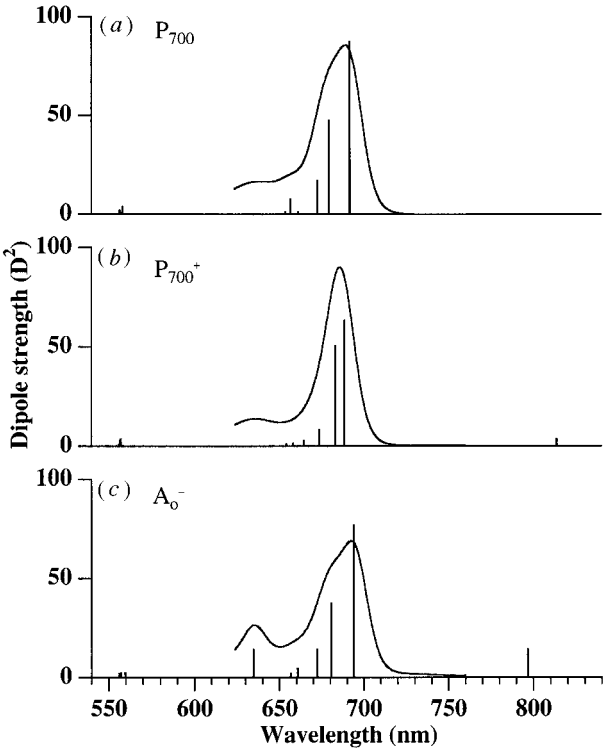

Figure 12. Calculated stick and broadened spectra of (*a*) the PSI, RC, (*b*) the RC with P_{700}^{+} and (*c*) with A_0^{-}. The calculated spectra were broadened by using the spectrum of Chl (Shipman & Housman 1979) centred at the appropriate energy eigenvalue and scaled with the dipole strength and according to the eigenvectors of equation (5.8). The Q_x transitions are at approximately 588 nm the lowest Chl^{+} and Chl^{-} transitions at 815 and 795 nm, respectively.

of the sixth pigment at the end of the structure is reduced and the other five are largely unaffected.

The coupling between $P1$ and $P2$ (table 2) is, surprisingly, almost the smallest value obtained as these molecules are rotated in their plane, i.e. about their z-axis, but the transition strength is close to being maximized. As coupling increases to a maximum of approximately 1200 cm^{-1} at about 200° between the Q_y dipoles, the transition is red-shifted but loses intensity and here tends to zero. Table 3 gives the final calculated angles between Q_y transitions in the RC as shown in figure 10.

8. Difference spectra

The data in figure 13(I) compare the experimental difference spectra at early time corresponding to $P_{700}^{+}A_0^{-}$–$P_{700}A_0$ and the calculated spectrum. The data have generally the same shape but the fit is poor, in part due to the noisy experimental data as it is the second difference, i.e. between transient difference spectra with and without a pre-flash. The calculated fit to the data for P_{700}^{+} and A_0^{-} difference spectra is far better. In P_{700}^{+}–P_{700}, figure 13(II) the calculated data have the same form as the picosecond experimental data (*b*), the bleaching transient at approximately 690 nm is reproduced well, but the smaller features at approximately 655 and 670 nm are at smaller wavelengths than observed experimentally. The P_{700}^{+}–P_{700} spectrum of

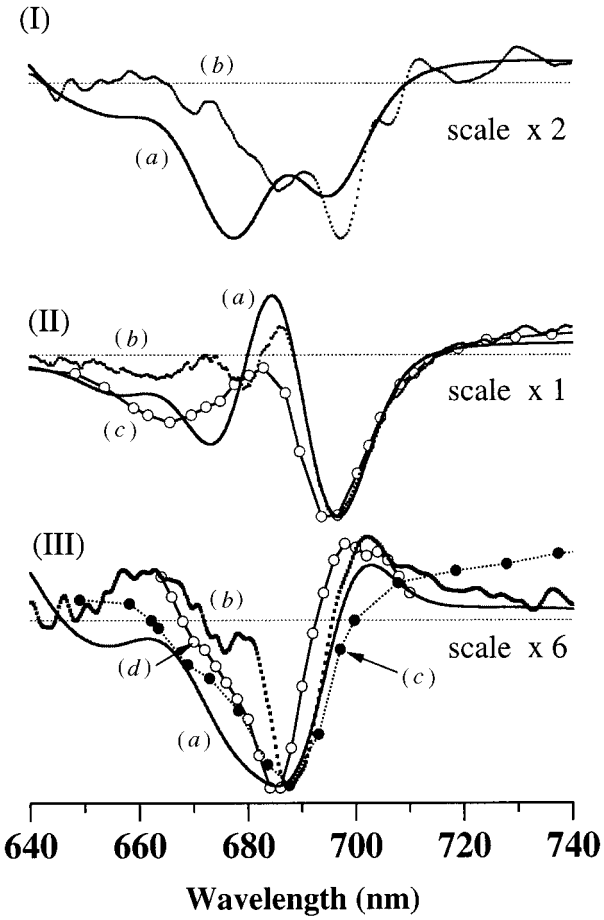

Figure 13. Calculated and experimental difference spectra (I) $P^{+}_{700}A^{-}_{0}$–A_0; (II) P^{+}_{700}–P_{700}; (III) A^{-}_{0}–A_0. The calculated spectra are the solid lines (*a*), the experimental (*b*) have been normalized to the peak absorption difference. In (II) the open circles are the P_{700} mutant data of Webber *et al.* (1996). In (III) the filled circles are from the data of Mathis *et al.* (1988) the open circles, Hastings *et al.* (1995). In (I) the experimental spectra (*b*) were measured at 1 ps after excitation in (II), at 500 ps and in (III) at 5 ps each by subtraction of the P^{+}_{700} spectrum from intermediate times as described by White *et al.* (1996).

Table 3. *Spherical polar angles, θ and ϕ (in degrees), for the Q_y dipoles and the geometry used to calculate figure 12*

	θ	ϕ
$P1$	66	−41
$P2$	75	137
$C3$	51	19
$C4$	52	170
$A5$	127	173
$A6$	141	1

θ is the angle from the z-axis, ϕ is measured from the x-axis (figure 10).

a mutant is also shown figure 13(II)*c*. In this mutant the histidine (*B*656), which interacts with one of the Chl of P_{700} (Webber *et al.* 1996), is replaced by either Asn or Ser. This small change has an effect mainly on the shorter wavelength band at approximately 667 nm but the whole spectrum is also slightly blue-shifted. Webber *et al.* suggest that either the 667 nm bleaching is due to P_{700}^{+} oxidizing a nearby Chl, or an altered excitonic interaction. The latter explanation is more consistent with our calculated data as this also has a bleach in the 660–680 nm region.

In the A_0^-–A_0 spectrum (figure 13(III)) the calculated and experimental data are in good agreement. The A_0^-–A_0 calculated spectrum is very sensitive to electrochromic effects. If these are not included a large bleaching occurs both at 680 and approximately 695 nm. A similar spectrum can also be reproduced by rotating the angles between $P1$ and $P2$ away from approximately 40° even when the electrochromic terms are included. The picosecond A_0^-–A_0 data (White *et al.* 1996*a*) (dotted line, figure 13(III)*b*) is the third difference and is narrower than the nanosecond data (filled circles) of Mathis *et al.* (1988) for reasons to do with the subtraction methods used in its generation. Figure 13(III)*d* shows the picosecond data of Hastings *et al.* (1995*a*) from detergent-treated spinach PSI particles. They have suggested that there may be a second transient in the A_0^-–A_0 spectrum, due to the other A_0 pigment (Hastings *et al.* 1995) if it is assumed that electron transfer is not unidirectional. This effect is expected to be seen in our model for although the coupling in P_{700} involves all molecules, to varying degrees, the different disposition of $A5$ and $A6$ does lead to slightly different A_0^- spectra depending on which of these molecules the electron is placed, but our simulations are not accurate enough to predict such a subtle effect.

9. Spectral simulations with disorder

The absorption spectra were also simulated satisfactorily by adding random perturbation energies to the elements of the exciton interaction matrix (equation (5.8)) and then using the numerical averaging method of Fidder *et al.* (Fidder *et al.* 1991; White *et al.* 1996*b*). These perturbation energies represent disorder and can be diagonal or off-diagonal where both can be either static or dynamic (Pope & Swenberg 1982). The ideal transition energies are represented by E_n, however, due to structural perturbations which cause static diagonal fluctuations, $\delta\varepsilon_{nn}$, these energies have a range of values and cause inhomogeneous broadening in the spectrum. The off-diagonal terms, δj_{nm}, represent the change in the interaction energy $J_{n,m}$, between molecules m and n compared to the 'perfect' structure. This fluctuation arises due to irregularity in positions or orientation of the molecules and contributes both to homogeneous and inhomogeneous line broadening,

$$\begin{bmatrix} \cdot\cdot & \cdot\cdot & \cdot\cdot & \cdot\cdot \\ \cdot\cdot & E_n + \delta\varepsilon_{n,n} + \delta\varepsilon^{\mathrm{t}}_{n,n} & J_{n,m} + \delta j_{n,m} + \delta j^{\mathrm{t}}_{n,m} & \cdot\cdot \\ \cdot\cdot & J_{m,n} + \delta j_{m,n} + \delta j^{\mathrm{t}}_{m,n} & \cdot\cdot & \cdot\cdot \\ \cdot\cdot & \cdot\cdot & \cdot\cdot & \cdot\cdot \end{bmatrix}.$$

There are also additional time-dependent fluctuations to the diagonal $\delta\varepsilon^{\mathrm{t}}_{nn}$ and off-diagonal $\delta j^{\mathrm{t}}_{nm}$ terms caused by phonons which describe the effect of protein (lattice) vibrations on the motion of the electron. In the dynamic off-diagonal case the transfer rate between molecules n and m is modulated by vibrations.

The magnitude of J_{nm} relative to the dynamic disorder, $\delta\varepsilon^{\mathrm{t}}$ and δj^{t}, and the static disorder energies, $\delta\varepsilon$ and δj, determine the main characteristics of the exciton

motion. If $J_{n,n+1}$ is by far the largest term the motion is band like with the usual extended Bloch states. If static disorder is large then variation in molecules positions or orientations leads to the range of transition energies ($E_n + \delta\varepsilon_{nn}$) and exciton transfer energies ($J_{nm} + \delta j_{nm}$) becoming important. If positional fluctuations are so large that they overcome the delocalizing effect of the average exciton coupling, $\langle J_{nm} + \delta j_{nm}\rangle_{\mathrm{av}}$ then localization occurs (Pope & Swenberg 1982), i.e. when $\langle \delta\varepsilon\rangle_{\mathrm{av}} > \langle J_{nm} + \delta j_{nm}\rangle_{\mathrm{av}}$.

Only static disorder was included in equation (5.8) and only the U^{ex} quadrant was used but with all four transitions on each of six pigments. An attempt to describe the effects of dynamic disorder is made below. To sample the energy distribution properly, 5000 matrices were diagonalized at each magnitude of the disorder. The spectra were satisfactorily fitted by adding diagonal disorder of 350 cm^{-1} and off-diagonal disorder of 100 cm^{-1}. These values are similar to, but larger than, those calculated for the LHII complex of *Rb. Sphaeroides* (230 and 110 cm^{-1}) (Jiminez *et al.* 1996). In PSII the diagonal disorder was calculated as 210 cm^{-1} (Durrant *et al.* 1995), however, hole burning studies on PSI, but at 1.6 K, indicate a inhomogeneous linewidth of 100 cm^{-1} (Gillie *et al.* 1989) far smaller than our estimate, possibly this result is caused by narrowing due to the exciton coupling.

The method of Fidder *et al.* (1991) can also be used to calculate the density of states, oscillator strength and localization of the coupled RC. As the standard deviation of the disorder, σ, becomes comparable to the electronic coupling, U, the eigenstates become localized and thus a measure of this localization is possible. The 'participation number', $L(E)^{-1}$, is such a measure and is defined as

$$L(E)^{-1} = N\rho(E)\left\langle \sum_j \delta(E - U_j) \sum_i a_{j,i}^4 \right\rangle^{-1}, \tag{9.1}$$

where $\rho(E)$ is the density of states at energy E, U_j the energy eigenvalue for state j and $a_{j,i}$ are the eigenvector coefficients for each molecule in that exciton state. The value of $L(E)^{-1}$ has consequences for the nature of the exciton state in the RC. Electronically isolated molecules would produce a value of one, coupled molecules with no disorder have a value of $\frac{2}{3}(N+1)$ or 4.67 for the $N = 6$ molecules in the RC. We find that as σ increases $L(E)^{-1}$ decreases as the exciton becomes more localized, and the average value over the band is empirically fitted at 100 cm^{-1} by a Lorentzian plus a constant:

$$\lambda(\sigma)^{-1} = a_1 + a_2/((\sigma - a_3)^2 + a_4),$$

with parameters $a_{1\ldots4} = 1.24,\ 6.52 \times 10^5,\ 237,\ 1.05 \times 10^5$, respectively. At $\sigma = 0$ the participation ratio is 4.8 very close to that predicted theoretically and falls to 1.2 at $\sigma = 3000\ \mathrm{cm}^{-1}$, essentially the single-molecule limit. At 350 cm^{-1} the participation is 2.7 indicating that the exciton has considerable delocalization, not only over the special pair but over at least three molecules or half the RC. This value of $L(E)^{-1}$ for the neutral RC is almost constant over the absorption band from approximately 640 to 680 nm but peaks slightly at approximately 690 nm. For P_{700}^{+} the participation is more symmetrical and decreases at the band edges to 2.0 from 2.4 in the band centre, this behaviour presumably reflecting the more localized nature of the exciton. The mean oscillator strength $\langle f\rangle_{\mathrm{av}}$ also varies across the absorption band, in the neutral RC it is constant below 660 nm then increases steadily from 0.15 to 1.5 at 690 nm, the lowest exciton states thus having gained oscillator strength. In P_{700}^{+} $\langle f\rangle_{\mathrm{av}}$ is

approximately 0.12 below 670 nm but then it rises rapidly to 1.15 at 680 nm which reflects the more localized nature of the exciton state.

As the molecules are coupled, the natural question to ask is for how long this coupling exists, or equivalently how quickly the localization occurs, as this will influence the subsequent electron-transfer processes. For example in a dimer the time for energy to transfer between the two molecules is $\tau_{\mathrm{el}} \sim \hbar/2\delta E$ which for a 300 cm^{-1} coupling is approximately 9 fs, but as time progresses the back and forth energy transfer will become out of phase as a result of intra- and inter-molecular vibrational motion or other interactions. If we take the time for these processes to be given by the corresponding experimental bandwidth of the P_{700} transition approximately 200 cm^{-1} this time is 13 fs, thus the coupling produced by the excitation process would be destroyed by motions of the protein matrix within very few transfer periods (Forster 1965). The coupling to the RC will have a range of strengths and frequencies which have not yet been determined experimentally in PSI. Hole-burning experiments generally show the phonon coupling of an antenna with the protein to be weak, whereas in the RC the electron–phonon coupling is large with a Huang–Rhys factor S of 4–6 compared to less than one in the antenna (Gillie *et al.* 1989). Measurements of the vibrational dephasing in the LHII antenna of 330 to approximately 460 fs (Joo *et al.* 1996) place an upper limit on this dephasing time. Using Mg tetraphenylporphyrin in THF, Galli *et al.* (1993) measured a similar time of 220 ± 13 fs for electronic dephasing. A lower limit to the dephasing time is obtained from photon echo experiments. In a strongly coupled system such as polyacetylene the echo decays in approximately 20 fs (Beddard *et al.* 1993), and in LHII a rapid 30 fs followed by a slower 530 fs decay is observed (Joo *et al.* 1996). The rapid decay is attributed to intramolecular vibrations and the ultrafast solvent mode, the slower one to inhomogeneity. Some of these times are longer than that of the simple estimate made above but it would seem clear that electronic dephasing of the PSI RC exciton state occurs well before electron transfer, which takes approximately 1 ps.

Initially the 'special pair' referred to the absorption maximum thought to be due to a pair of molecules. A better description of the absorption is that it is due to an exciton coupled state covering initially six chromophores but which is partly localized by disorder and by inter- and intra-molecular vibrations to three. More detailed information on the electronic structure of the PSI RC might be obtained from experiments done with femtosecond resolution in the infrared. As an example, in bacterial RC from *Rb. Sphaeroides* a sharp band at 2710 cm^{-1} and a broad band at approximately 5300 cm^{-1} has been observed (Wynne *et al.* 1996). It has been suggested (Scherer & Fischer 1997) that the 2710 cm^{-1} band arises from a transition from $P^* \rightarrow P^{**}$, where P^{**} is a singlet component of a doubly excited state and also that the transition intensity is enhanced by nearby CT states.

10. Conclusions

Some parameters defining the energy migration properties of photosynthetic antennae are discussed. In particular it is shown that when Chl molecules are closer than approximately 5 Å, in their plane–to–plane separation, states with a large charge-transfer character are lower than exciton states and this could lead to excited state quenching. This is put to advantage in the P_{700} RC where only the molecules of the special pair are close enough to produce a lowest CT state.

The X-ray geometry of PSI has been used to model both energy migration and

exciton coupling in the PSI reaction centre antenna protein. The energy migration was found to be trap limited as did a calculation on a smaller antenna. The intrinsic rate constant for energy transfer at approximately $1.3\,\mathrm{ps}^{-1}$ is slightly larger than calculated previously (White *et al.* 1996*a*). Exciton coupling in the RC shows that the experimental P_{700}^{+}–P_{700} and A_0^{-}–A_0 spectra are well described by using the X-ray geometry provided the molecules are rotated in their plane. The exciton coupling does not vary much between near neighbours in the RC and is approximately $300\,\mathrm{cm}^{-1}$ and no especially large coupling between the molecules $P1$, $P2$ of the special pair is needed to describe the spectra. Electrochromic effects are important and greatly influence the shape of the A_0^{-}–A_0 difference spectrum.

I am most grateful to Dr N. Krauss for providing the PSI X-ray coordinate data before publication, and for many helpful discussions with Dr Peter Heathcote and Dr Gavin Reid, and also to Dr Jo McDouall for the Gaussian 94 calculations. The support of the BBSRC, EPSRC and the Royal Society is acknowledged.

References

Alden, R. G., Parson, W. W., Chu, Z. T. & Warshel, A. 1995 *J. Am. Chem. Soc.* **117**, 12 284–12 298.

Alden, R. G., Parson, W. W., Chu, Z. T. & Warshel, A. 1995 *J. Phys. Chem.* **100**, 16 761–16 770.

Beddard, G. S., Carlin, S. & Porter, G. 1976 *Chem. Phys. lett.* **43**, 27–30.

Beddard, G. S., Feehan, T. M., Keyes, T. E., Reid, G. D., Thorne, J. R. G., White, N. T. & Heathcote, P. 1995 Excitation transfer in ψ. In *Femtochemistry* (ed. M. Chergui), pp. 394–400. Singapore: World Scientific.

Beddard, G. S., McFadyen, G. G., Reid, G. D. & Thorne, J. R. G. 1993 *Chem. Phys.* **172**, 363.

Beddard, G. S. & Porter, G. 1976 *Nature* **260**, 366–367.

Breton, J., Martin, J.-L., Fleming, G. & Lambry, J.-C. 1988 *Biochemistry* **27**, 8276–8284.

Chow, H., Serlin, R. & Strouse, C. E. 1974 *J. Am. Chem. Soc.* **97**, 7230–7237.

Deisenhofer, J. & Michel, H. 1989 *Angew. Chem. Int. Ed. Engl.* **28**, 829–847.

Deisenhofer, J.,, Epp, O., Kiki, K., Huber, R. & Michel, H. 1984 *J. Mol. Biol.* **180**, 385–398.

Durrant, J. R., Klug, D. R., Kwo, S. L., Grondelle, R. v., Porter, G. & Dekker, J. P. 1995 *Proc. Natn. Acad. Sci. USA* **92**, 4798–4802.

Falk, J. E. 1964 *Porphyrins and mettaloporphyrins*. New York: Elsevier.

Feick, R. & Fuller, R. C. 1984 *Biochemistry* **32**, 3693–3700.

Fenna, R. E. & Matthews, B. W. 1977 *Brookhaven Symposium: biology* vol. 28, pp. 170–182. Springfield: U.S. Department of Commerce.

Fidder, H., Knoester, J. & Wiersma, D. A. 1991 *J. Chem. Phys.* **95**, 7880–7890.

Forster, T. 1965 Delocalized excitations. In *Modern quantum chemistry* (ed. O. Sinanoglu), vol. III, pp. 93–137. New York: Academic.

Frisch, M. J. (and 30 others) 1995 *Gaussian 94*. Pittsburg: PA: Gaussian Inc.

Fromme, P. 1996 *Curr. Opinion Struct. Biol.* **3**, 473–484.

Fromme, P., Witt, P., Schubert, W. D., Klukas, O., Saenger, W. & Krauss, N. 1996 *Biochem. Biophys. Acta* **1275**, 76–83.

Fujita, I., Davis, M. S. & Fajer, J. D. 1978 *J. Am. Chem. Soc.* **100**, 6280–6282.

Galli, C., Wynne, K., LeCours, S. M., Therien, M. J. & Hochstrasser, R. M. 1993 *Chem. Phys. Lett.* **206**, 493–499.

Gantt, E., Lipschultz, C. A. & Zilinskas, B. A. 1977 In *Brookhaven Symposium: chlorophyll proteins, reaction centres and photosynthetic membranes* (ed. G. H. J. Olsen), vol. 28, pp. 347–357. Springfield: US Department of Commerce.

Gillie, J. K., Lyle, P. A., Small, G. J. & Goldbeck, J. H. 1989 *Photosynth. Res.* **22**, 233–246.

Gouterman, M. 1978 Optical spectra and electronic structra of porphyrins and related rings. In *The porphyrins*. New York: Academic.

Grondelle, R. v. 1985 *Biochim. Biophys. Acta* **811**, 147–195.

Haran, G., Wynne, K., Moser, C. C., Dutton, P. L. & Hochstrasser, R. M. 1996 *J. Phys. Chem.* **100**, 5562–5569.

Hastings, G., Durrant, J. R., Barber, J., Porter, G. & Klug, D. R. 1992 *Biochem.* **31**, 7638–7647.

Hastings, G., Hoshina, S., Webber, A. N. & Blankenship, R. E. 1995*a* *Biochem.* **34**, 15 512–15 522.

Hastings, G., Reed, L. J., Lin, S. & Blankenship, R. E. 1995*b* *Biophys. Jl* **69**, 2044–2055.

Hemenger, R. P., Lakatos-Lindenberg, K. & Pearlstein, R. 1972 *J. Math. Phys.* **13**, 1056–1063.

Holzwarth, A. R., Schatz, G. H., Brock, H. & Bittersman, E. 1993 *Biophys. Jl* **64**, 1813–1826.

Hu, X., Ritz, T., Damjanovic, A. & Shulten, K. 1997 *J. Phys. Chem* B **101**, 3854–3871.

Huber, R. 1989 *Angew. Chem. Int. Ed. Engl.* **28**, 848–869.

Jia, Y., Jean, J. M., werst, M. M., Chan, C.-K. & Fleming, G. R. 1992 *Biophys. Jl* **63**, 259–273.

Jiminez, R., Dikshit, S. N., Bradforth, S. E. & Fleming, G. R. 1996 *J. Phys. Chem.* **100**, 6825–6834.

Joo, T., Jia, Y., Yu, J.-Y., Jonas, D. & Fleming, G. R. 1996 *J. Phys. Chem.* **100**, 2399–2409.

Kalinowski, J., Giro, G., DiMarco, P., Camaioni, N. & Fattori, V. 1997 *Chem. Phys. lett.* **265**, 607–613.

Kamagowa, K., Morris, J., Takagi, Y., Nakashima, N., Yoshihara, K. & Ikegami, I. 1983 *Photochem. Photobiol.* **37**, 207.

Koepke, J., Hu, X., Muenke, C., Shulten, K. & Michel, H. 1996 *Structure* **4**, 581.

Krauss, N., Hinrichs, W., Witt, W., Fromme, P., Pritzkow, W., Dauter, Z., Betzel, B., Wilson, K. S., Witt, H. & Saenger, W. 1993 *Nature* **361**, 326–331.

Krauss, N., Schubert, W. D., Klukas, O., Fromme, P., Witt, H. T. & Saenger, W. 1996 *Nature Struct. Biol.* **3**, 965–973.

Kuhlbrandt, W., Wang, D. N. & Fujiyoshi, K. 1994 Nature **367**, 614–621.

Kumazaki, S., Kandori, H., Petek, H. & Yoshihara, K. 1994 *J. Phys. Chem.* **98**, 10 335–10 342.

Kwa, S. L. S., Eijckelhoff, C., Grondelle, R. v. & Dekker, J. P. 1994 *J. Phys. Chem.* **98**, 7702.

Lee, J. W., Lee, I., Laible, P. D., Owens, T. G. & Greenbaum, E. 1995 *Biophys. Jl* **69**, 652–659.

Lin, S., Kleinherenbrink, F. A., Chiou, H.-C. & Blankenship, R. E. 1994 *Biophys. Jl* **67**, 2479–2489.

MacDermott, G., Prince, S. M., Freer, A. A., Hawthornthwaite-Lawless, A. M., Papiz, M. Z., Cogdell, R. J. & Isaacs, N. W. 1995 *Nature* **374**, 517.

Markovitski, D., Lecuyer, I., Lianos, P. & Malthete, J. 1991 *J. Chem. Soc. Faraday Disc.* **87**, 1785–1790.

Mathis, P., Ikegami, I. & Setif, P. 1988 *Photosynth. Res.* **16**, 203–210.

Mourik, F. v., Verwijst, R. R., Mulder, J. M. & Grondelle, R. v. 1994 *J. Phys. Chem.* **98**, 10 307–10 312.

Nagashima, U., Takada, T. & Ohno, K. 1986 *J. Chem. Phys.* **85**, 4524–4529.

Noort, P. v., Zhu, Y., LoBrutto, R. & Blankenship, R. E. 1997 *Biophys. Jl* **72**, 316–325.

Owens, T. G., Webb, S. P., Alberte, R. S. & Fleming, G. R. 1987 *Proc. Natn. Acad. Sci. USA* **84**, 1532–1536.

Owens, T. G., Webb, S. P., Alberte, R. S., Mets, L. & Fleming, G. R. 1988 *Biophys Jl* **53**, 733–745.

Parson, W. W. & Warshel, A. 1987 *J. Am. Chem. Soc.* **109**, 6152–6163.

Pearlstein, R. 1982 *Photochem. Photobiol.* **35**, 835–844.

Petke, J. D., Maggiora, G. M., Shipman, L. L. & Christoffersen, R. E. 1978 *J. Mol. Spec.* **73**, 311–331.

Pope, M. & Swenberg, C. E. 1982 *Electronic processes in organic crystals*. Oxford University Press.

Renge, I. 1993 *J. Phys. Chem.* **97**, 6582–6589.

Sauer, K., Lindsay-Smith, J. R. & Schultz, A. J. 1966 *J. Am. Chem. Soc.* **88**, 2681.

Savikhin, S., Zhou, W., Blankenship, R. & Struve, W. 1994 *Biophys. Jl* **66**, 110–114.

Scherer, P. O. J. & Fischer, S. F. 1989 *J. Phys. Chem.* **93**, 1633–1637.

Scherer, P. O. J. & Fischer, S. F. 1997 *Chem. Phys. Lett.* **268**, 133–142.

Seely, G. R. 1973 *J. Theor. Biol.* **40**, 189–199.

Shipman, L. & Housman, D. 1979 *Photochem. Photobiol.* **29**, 1163.

Shubin, V. V., Bezsmertnaya, I. & Karapetyan, N. V. 1995 *J. Photochem. Photobiol.* B **30**, 153–160.

Shuvalov, V. A., Nuijs, M. J., Gorkom, H. K. v., Smit, H. W. & Duysens, L. M. 1986 *Biochim. Biophys. Acta* **850**, 319–323.

Small, G. J. 1995 *Chem. Phys.* **197**, 239–257.

Thompson, M. A. & Zerner, M. 1991 *J. Am. Chem. Soc.* **113**, 8210–8215.

Thompson, M. A. & Schenter, G. K. 1995 *J. Phys. Chem.* **99**, 6374.

Thompson, M. A., Zerner, M. C. & Fajer, J. 1991 *J. Phys. Chem.* **95**, 5693.

Tronrud, D. E., Schmid, M. F. & Matthews, B. W. 1986 *J. Mol. Biol.* **188**, 443–454.

Turconi, S., Schweitzer, G. & Holzwarth, A. R. 1993 *Photochem. Photobiol.* **57**, 113–119.

Warshel, A., Chu, Z. T. & Parson, W. W. 1994 *J. Photochem. Photobiol.* A **82**, 123–128.

Wasielewski, M. R., Fenton, J. M. & Govindjee 1987 *Photosynth. Res.* **12**, 181–190.

Webber, A., Su, H., Bingham, S. E., Kass, H., Krabben, L., Kuhn, M., Jordan, R., Schlodder, E. & Lubitz, W. 1996 *Biochem.* **35**, 12 857–12 863.

Werst, M., Jia, Y. & Fleming, G. 1992 *Biophys. Jl* **61**, 868–878.

White, N., Beddard, G. S., Thorne, J. R. G., Feehan, T., Keyes, T. & Heathcote, P. 1996*a* *J. Phys. Chem.* **100**, 12 086–12 099.

White, N., Feehan, T. M., Thorne, J. R. G., Beddard, G. S. & Heathcote, P. 1996*b* Aspects of excitation transfer. In *54th Int. Meeting of Phys. Chem., Fast Elementary Processes in Chemistry and Biology* (ed. A. Tramer), vol. 364, pp. 218–287. New York: AIP.

Wynee, K., Haran, G., Reid, G. D., Moser, C. C., Dutton, P. L. & Hochstrasser, R. M. 1996 *J. Chem. Phys.* **100**, 5140–5148.

Zandvoort, M. A. M. v., Wrobel, D., Lettinga, P., Ginkel, G. v. & Levine, Y. K. 1995 *Photochem. Photobiol.* **62**, 299–308.

Zinth, W., Knapp, E. W., Fischer, S. F., Kaiser, W., Diesenhofer, J. & Michel, H. 1995 *Chem. Phys. Lett.* **119**, 1.

Zuber, H. 1986 *TIBS* **11**, 414–419.